



# Surface adsorption configurations of H<sub>3</sub>PO<sub>4</sub> modified TiO<sub>2</sub> and its influence on the photodegradation intermediates of gaseous o-xylene

Zhuang Wang<sup>a,b</sup>, Asad Mahmood<sup>a</sup>, Xiaofeng Xie<sup>a,\*</sup>, Xiao Wang<sup>a</sup>, Hanxun Qiu<sup>b</sup>, Jing Sun<sup>a</sup>

<sup>a</sup> The State Key Lab of High Performance Ceramics and Superfine Microstructure, Shanghai Institute of Ceramics, Chinese Academy of Sciences, 1295 Dingxi Road, Shanghai 200050, China

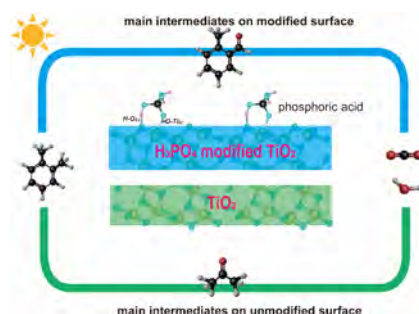
<sup>b</sup> School of Material Science and Engineering, University of Shanghai for Science and Technology, 516 Jungong Road, Shanghai 200093, China

## HIGHLIGHTS

- The most stable adsorption mode of phosphoric acid on anatase TiO<sub>2</sub> (101) surface is demonstrated.
- Phosphoric acid modified TiO<sub>2</sub> shows a remarkable photocatalytic activity.
- The main intermediates of gaseous o-xylene degradation on PT0 and PT1 surface are identified.
- The influence of surface phosphoric acid on photodegradation intermediates of gaseous o-xylene is proposed.

## GRAPHICAL ABSTRACT

H<sub>3</sub>PO<sub>4</sub> adsorbed on TiO<sub>2</sub> by forming H–O<sub>2</sub>C and =O–Ti<sub>5</sub>C bonds, further change o-xylene adsorption configuration to favor its methyl oxidation.



## ARTICLE INFO

### Keywords:

Photocatalysis  
TiO<sub>2</sub>  
Phosphoric acid  
VOCs degradation  
O-xylene

## ABSTRACT

For the oxide-based photocatalysts, polyoxylic acid modification can affect their adsorption/desorption properties and further regulate photocatalytic reaction pathway, which is crucial for enhancing photocatalytic activity and selectivity. Herein, phosphoric acid modified TiO<sub>2</sub> was synthesized by a facile impregnation-calcination method for photocatalytic degradation of gaseous o-xylene. According to FTIR, XPS, and EDS analysis, phosphoric acid was anchored on the surface of TiO<sub>2</sub> successfully. The surface P atomic percentages for PT1 was 2.45%. The as-prepared phosphoric acid modified TiO<sub>2</sub> (PTx) had a photocatalytic performance superior to that of commercial TiO<sub>2</sub> and unmodified TiO<sub>2</sub> (PT0), with increasing by 2.2 times at most. Interestingly, the phosphoric acid molecules strongly adsorbed on anatase TiO<sub>2</sub> surface by forming H–O<sub>2</sub>C and =O–Ti<sub>5</sub>C chemical bonds according to the first principle calculations, which changed TiO<sub>2</sub> surface properties (specific surface area and surface negative electrostatic field) and further improved adsorption and charge carrier separation and transfer, thus improving the photocatalytic activity. Additionally, according to the intermediates results, the relative abundance of intermediates shows obvious difference. Acetone was detected as the most abundant intermediates during o-xylene degradation for PT0, whereas that was o-methyl benzaldehyde for PT1, which could be ascribed to the difference of surface adsorption configuration of o-xylene. According to the temperature-programmed desorption (TPD) results, the surface modified by phosphoric acid could change the o-xylene adsorption configuration to favor its methyl oxidation (standing configuration), whereas the unmodified surface could be more favorable to the benzene ring-open reaction (lying configuration). This work will deepen the

\* Corresponding author.

E-mail address: [xxfshcn@163.com](mailto:xxfshcn@163.com) (X. Xie).

<https://doi.org/10.1016/j.cej.2020.124723>

Received 21 November 2019; Received in revised form 4 March 2020; Accepted 7 March 2020

Available online 10 March 2020

1385-8947/ © 2020 Elsevier B.V. All rights reserved.

understanding of the relevance of surface modification and surface photocatalytic reaction, which also provides a feasible strategy to improve photocatalytic selectivity.

## 1. Introduction

Over the last few decades, environmental problems, especially air pollution, have seriously threatened human health [1–3]. Volatile organic compounds (VOCs) represent an important class hazardous air pollutant, of which most are considered potentially mutagenic and carcinogenic to human beings [4,5]. Up to now, some conventional treatment techniques including adsorption [6,7], membrane separation [8], thermal catalysis [9,10], ozone oxidation [11], biological purification [12], and plasma treatment [13,14] are widely applied to eliminate VOCs, but some of them are nondestructive and need high energy consumption. Recently, photocatalytic oxidation (PCO), efficient and environmentally friendly, has been increasingly used to removal VOCs [15–17].

For expanding the applications of PCO technology, high efficiency and selectivity, long lifetime and low-cost photocatalyst materials are desired. Titanium dioxide is always considered as the most promising candidate among many photocatalysts. To advance this promising photocatalyst, various modification strategies were proposed [18–24]. Moreover, many previous works were proposed on photocatalyst preparation and modification for removal of VOCs. Matsuda et al. [25] used a sol-gel method and treated with polyethylene glycol to prepare a transparent porous anatase-type nanocrystalline silicon dioxide film, which had higher photocatalytic degradation activity for removal gaseous acetaldehyde. Zhang et al. [26] prepared Ag/AgBr/TiO<sub>2</sub> composites by a deposition precipitation method, which was mainly used for photocatalytic degradation of VOCs. It is more stable under ultraviolet and visible light, and has better photocatalytic efficiency for benzene, acetone, etc. than P25. Jo et al. [27] prepared nitrogen-doped N-TiO<sub>2</sub> and evaluated the photocatalytic degradation ability of modified and unmodified pure TiO<sub>2</sub> for VOCs. The four target gases (ethylbenzene, p-xylene, m-xylene, o-xylene), the degradation rate of the ring reactor coated with N-TiO<sub>2</sub> materials are higher than 90%, which is significantly better than the degradation efficiency of the reactor coated with TiO<sub>2</sub>. A.H. Mamaghani et al. [28] developed a novel hydrothermal route to synthesize crystalline and hierarchically porous TiO<sub>2</sub> under acidic/basic reaction environment for MEK degradation and investigated the effect of photocatalyst features (crystallinity, surface area, crystal size, OH population, and porosity) and operation parameters (inlet concentration, airflow rate, and relative humidity) on photocatalytic activity, which suggested the importance of finding the best balance between surface area, crystal size, crystallinity, OH density, and meso-porosity to optimize the photoactivity. These preparation and modification methods for removal of VOCs either have complicated and time-consuming steps or have ambiguous mechanism on degradation intermediates and structure-property relationship. Surface modification by inorganic acid was considered as a facile, effective method to improve photocatalytic activity of TiO<sub>2</sub> for degrading VOCs. On the one hand, surface acid modification will avoid the light shielding effect caused by composites. On the other hand, the surface acid modification method is simple and efficient, and it is more favorable to degrade gaseous pollutants than aqueous pollutants because surface complex could be easily attacked by water molecules and further desorbs in the liquid phase, which can be avoided in the gas phase [29,30]. It was reported that phosphate, widely present in the natural world, can adsorb strongly on the surface of TiO<sub>2</sub> by surface complex, which can greatly influence the interfacial and surface chemistry of TiO<sub>2</sub> [31]. Hence, phosphoric acid was chosen as phosphate source to modify TiO<sub>2</sub>. There have been many previous reports focusing on phosphoric acid surface modification. For example, Jung won Kim et al. [32] reported that surface modified TiO<sub>2</sub> (P-TiO<sub>2</sub>/Pt) was prepared by a simple two-step method using phosphoric acid (as phosphate source) and chloroplatinic acid (as platinum source). P-TiO<sub>2</sub>/Pt showed a significantly higher photocatalytic

activity than any of bare TiO<sub>2</sub>, P-TiO<sub>2</sub>, and Pt/TiO<sub>2</sub> for the degradation of phenolic compounds. The authors also pointed out that the surface phosphoric acid modification that replace the surface hydroxyl groups on TiO<sub>2</sub> favored the formation of unbound OH radicals instead of surface-bound OH radicals. Qin et al. [33] modified Degussa P25 TiO<sub>2</sub> with the phosphoric acid and showed the surface modification improved the thermal stability which was closely related to the inhibition effect of phosphate group on the surface mass diffusion as well as the directing connection of TiO<sub>2</sub> nanoparticles. Bai et al. [34], Chen et al. [35] and Cui et al. [36] suggested surface acid treatment not only influenced the morphology and structure properties, but also modulated electrons capture by promoting O<sub>2</sub> adsorption. Wu et al. [37] co-modified residual chlorine rutile TiO<sub>2</sub> nanorods with phosphoric and boric acids and tested the photocatalytic activity towards gas-phase acetaldehyde and liquid-phase phenol. The authors confirmed the targeted co-modification could greatly promote the capture of the photogenerated electrons, thus improving the photocatalytic activity. Hence, based on the previous reports, few studies focused on how phosphoric acid adsorbed on the surface at the molecular level and what the influence of modified surface on the photodegradation intermediates is, which is crucial for understanding the relationship between surface acid modification and surface photodegradation reaction. During VOCs photodegradation reaction, given the short residence time of reactants and adsorption competition, many oxidation intermediates are generated [38,39]. In fact, generation of intermediates is one of the main concerns associated with PCO application since some of these intermediates can be even more toxic than their parent compounds [40,41]. O-xylene, a typical aromatic VOC, is delivered to the atmosphere via natural and industrial operations [42,43], also used as a solvent and cleaning agent in different industrial process. The o-xylene derivatives might cause headache, dizziness, kidney and coronary disease, exhaustion. Therefore, it is critical to eliminate o-xylene in the indoor air environment and investigate their oxidation intermediates mechanism.

The objective of this work is helping the targeted design of TiO<sub>2</sub>-based photocatalyst by understanding of how phosphoric acid adsorbed on the surface at the molecular level and what the influence of modified surface on the photodegradation intermediates is. Herein, phosphoric acid modified TiO<sub>2</sub> was synthesized by a facile impregnation-calcination method for photocatalytic degradation of gaseous o-xylene. The different adsorption configurations and corresponding LDOS and electron density difference (EDD) were calculated for understanding the adsorption mode of phosphoric acid and its influence on the surface. The as-prepared phosphoric acid modified TiO<sub>2</sub> (PTx) had a photocatalytic performance superior to that of commercial TiO<sub>2</sub> and unmodified (PT0). Moreover, possible surface reaction process on both surfaces was proposed.

## 2. Experimental

### 2.1. Chemicals and materials

Commercial titanium dioxide (TiO<sub>2</sub>, Anatase) was purchased from Aladdin Industrial Corporation. Phosphoric acid (H<sub>3</sub>PO<sub>4</sub>, wt% ≥ 85%) was purchased from Sinopharm Chemical Reagent Co., Ltd. Absolute ethanol was supplied by Shanghai Zhenxing Co., Ltd. Deionized (DI) water was produced by a Milli-Q system (R > 18.1MΩ). P-benzoquinone (PBQ) and 2,2,6,6-tetramethyl-1-piperidinyloxy (TEMPO) were purchased from Aladdin Industrial Corporation. All chemicals used in our study were of analytical grade and used without further purification.

## 2.2. Synthesis of phosphoric acid modified TiO<sub>2</sub>

Briefly, 0.5 g of commercial TiO<sub>2</sub> was added into a plastic bottle containing 5 mL absolute ethanol and 25 milling balls. Then it was milled for 24 h, marked as suspension A. At the same time, an appropriate amount of phosphoric acid was added into a beaker containing 25 mL deionized water, followed by stirring for 2 h, marked as solution B. Then suspension A was dropped into solution B, with the mixed suspension stirring for 2 h. After that, the mixed suspension was centrifuged and washed by deionized water several times until the pH of supernatant was 7 or neutral, and then dried at 80 °C. Then the sample was heated to 450 °C at a heating rate of 5 °C/min, kept at 450 °C for 0.5 h, and then naturally cooled to room temperature in a muffle furnace to obtain phosphoric acid modified TiO<sub>2</sub>. The samples were denoted as PT<sub>x</sub>, where x represented the mass ratio of added phosphoric acid and TiO<sub>2</sub>. Commercial TiO<sub>2</sub> was also used for comparison. Here, the commercial TiO<sub>2</sub> is anatase TiO<sub>2</sub> without any further treatment, purchased from Aladdin Industrial Corporation. The PT0 is prepared by impregnation-calcination method without adding phosphorous acid, using commercial TiO<sub>2</sub>.

## 2.3. Characterization

The morphologies, nanostructures and composition of samples were observed by Field Emission Scanning Electron Microscope (FE-SEM, Magellan 400) and Transmission Electron Microscope (TEM, FEI Electron Optics, Tecnai G2 F20). The elemental mapping analysis was determined using Energy Dispersive Spectrometer (EDS). X-ray diffraction (XRD) were carried out on a high-resolution powder X-ray diffractometer (BRUKER AXS GMBH, D8 ADVANCE) using Cu K $\alpha$  radiation ( $\lambda = 0.15418$  nm,  $2\theta$  varied from 20° to 80°, 8°/min). Fourier transform infrared (FTIR) spectra were collected by a ThermoFisher iN10 iZ10 infrared spectrophotometer with a KBr pellet technique. X-ray photoelectron spectroscopy (XPS) and valence band XPS (VB-XPS) experiments were carried out on a RBD upgraded PHI-5000C ESCA system (Perkin Elmer) with MgK $\alpha$  radiation (1253.6 eV). Raman spectra were collected by a DXR Raman Microscope using a laser with an excitation wavelength of 532 nm at laser power of 7 mW (Thermal Scientific Corporation, USA). The Brunauer–Emmett–Teller (BET) specific surface area of the samples was measured by a Micromeritics ASAP 3000 nitrogen adsorption apparatus (All the samples were degassed at 120 °C for 5 h before nitrogen adsorption measurements were taken). UV-vis diffuse reflectance spectra were obtained on a Shimadzu UV-3600 spectrometer by using BaSO<sub>4</sub> as reference. Photoluminescence (PL) spectra were tested at room temperature by an Edinburgh Instruments FLSP-920 fluorescence spectrophotometer with an excitation wavelength of 320 nm. Photocurrent response and electrochemical impedance characterization were carried out on a CHI 660D electrochemical workstation with a conventional three-electrode quartz cell. The working electrodes were prepared by coating sample suspension (containing 50 mg sample and 2 mL absolute ethanol) onto the cleaned FTO glass (1.0 \* 2.5 cm). Platinum plate and Ag/AgCl electrode were used as counter electrode and reference electrode, respectively. Photocurrent response for the electrodes were measured under 0.2 V versus Ag/AgCl. NaCl solution (100 mL, 1 mol/L) was used as an electrolyte solution. An AM1.5G solar power system was used as light irradiation source. Electrochemical impedance spectra (EIS) were measured by applying 5 mV alternative signal versus the reference electrode over the frequency range of 0.1 Hz–1 MHz. The 100 mL of 0.1 mol/L KCl, 1 mmol/L Fe(CN)<sub>2</sub> and Fe(CN)<sub>3</sub> was utilized as an electrolyte solution. Electron spin resonance (ESR) signals of radicals ( $\cdot$ OH and  $\cdot$ O<sub>2</sub><sup>-</sup>) spin-trapped by 5,5-dimethyl-1-pyrroline N-oxide (DMPO) in water or ethanol were detected by a JES-FA200 spectrometer. Temperature-programmed desorption (TPD) measurements of photocatalysts were conducted on ChemiSorb PCA-1200 instrument (Builer, China). Briefly, sample powder (0.1 g) was pretreated in a

quartz tube at 120 °C for 1 h under a high-pure N<sub>2</sub> flow, and then the temperature was cooled to 30 °C. For gaseous o-xylene adsorption saturation, the sample was continuously blown with 50 ppm o-xylene for 2 h at 30 °C. After adsorption, the sample was flushed with high-pure N<sub>2</sub> flow to remove the physically adsorbed o-xylene on the powders. An o-xylene-TPD profile of the sample was recorded by increasing the temperature from 30 °C to 800 °C at a heating rate of 10 °C/min under high-pure N<sub>2</sub> flow.

## 2.4. Photocatalytic experiments and intermediates detection

Photocatalytic degradation experiments of gaseous o-xylene were carried out on a continuous, automated, gas flow photocatalytic real-time test system equipped with a gas mixer, a cuboid reactor (15 \* 8 \* 1 cm) and gas chromatograph (Fig. S1). First, 0.1 g sample was mixed with 10 mL ethanol, and then the suspension was doctor-blade coated on glass plate (12 \* 5 cm), which was placed into a reaction chamber and sealed with a quartz glass. Then 25 ppm o-xylene flowed through the reaction chamber at a flow rate of 40 mL/min. The residence time was calculated to be 2.4 min (residence time = 120 mL/40 mL/min \* 12 cm/15 cm = 2.4 min). After the adsorption–desorption equilibrium between gaseous o-xylene and photocatalyst surface was established in the dark for 2.5 h, the lamp was turned on. Herein, a 300 W xenon lamp was utilized to provide simulated sunlight irradiation with a light density of 80 mW/cm<sup>2</sup> measured with THORLABS GmbH (PM100D; S314C detector). And the distance between sample and irradiation source was ca. 30 cm. Finally, the concentrations of o-xylene during the photocatalytic degradation process were monitored by a gas chromatography (equipped with a flame ionization detector). The degradation efficiency of o-xylene was calculated by using the formula:  $(1 - C/C_0) \times 100\%$ , where C<sub>0</sub> was the initial concentration and C was the concentration of o-xylene at different time intervals. The intermediate products of photocatalytic degradation of gaseous o-xylene were identified by a gas chromatography-mass spectrometer (Thermo Fisher Scientific, TSQ 8000 Evo). Before the GC-MS analysis, the PT0 and PT1 sample powder collected after 240 mins photocatalytic reaction was heated at 200 °C for 5 min. Gaseous intermediates desorbed from the surface were analyzed by GC-MS. The column temperature program of GC was set as follows: the initial temperature was 35 °C for 3 min, then increased up to 280 °C and remained at this temperature for 3 min. The injector temperature was 280 °C. Helium was used as the carrier gas. Mass spectrometric detection was operated with 70 eV electron impact (EI) mode and the ionization temperature was 250 °C. The scavenger experiment was the same as photocatalytic experiment. The difference was that the scavenger experiment needed to add ROS scavenger (2,2,6,6-tetramethylpiperidine oxide, TEMPO,  $\cdot$ OH scavenger and p-benzoquinone, PBQ,  $\cdot$ O<sub>2</sub><sup>-</sup> scavenger) during the photocatalytic test. During the test, 0.01 g TEMPO or PBQ was mixed with 0.1 g photocatalyst in ethanol, then the mixture was drip-coated onto a dry glass plate for scavenger experiments.

## 2.5. Theoretical calculation details

The first principle calculations were carried out using Vienna Ab-initio Simulation Package (VASP) [44,45]. The Generalized Gradient Approximation (GGA) exchange correlation function given by Perdew-Burke-Erzenhof was used for the geometry optimizations and properties calculations [46]. Initially, the bulk TiO<sub>2</sub> was fully relaxed in a 2 \* 2 \* 2 supercell. The optimized lattice parameters were calculated as a = b = 3.778 Å, c = 9.491 Å;  $\alpha = \beta = \gamma = 90.00^\circ$ , which are in close agreement with the experimental values [47,48]. A 4 \* 4 \* 1 k-point set was used along with 400 eV as cutoff energy. An ultra-soft pseudopotential was used during all calculations. Next, the optimized bulk structure of TiO<sub>2</sub> was cleaved along the (101) direction to create a slab model. The surface model contained 158 number of atoms including 64 Ti and 94 oxygen atoms. The thickness of the surface was



calculated as 13.14 Å. A vacuum of 20 Å was used to avoid the interaction of the self-mirror reflection's during calculations. A  $1 \times 2 \times 1$  k-point set was used as for the surface calculations. The cutoff energy was 400 eV for all calculations. Additionally, a pairwise force field DFT-D2 was used to describe the weak non-covalent van der Waals interactions accounted in Grimme function [49]. The lattice was relaxed until the maximum force and displacement was 0.03 eV/Å and 0.001 Å, respectively. The electronic configurations of the atoms used are as follows: for surface Ti: [Ne] 3s<sup>2</sup> 3p<sup>6</sup>; O: [He] 2s<sup>2</sup> 2p<sup>6</sup>; for molecule P: [Ne] 3s<sup>2</sup> 3p<sup>3</sup>; O: [He] 2s<sup>2</sup> 2p<sup>4</sup>; H:1s<sup>1</sup>. Additionally, the bottom four layers were fixed to imitate bulk, while the surface layers were allowed to relax during the calculations. Different configurations of the phosphoric acid molecules were used to find the most stable adsorption complex. The following equation was used for the adsorption energy calculations.

$$E_{\text{ads}} = E_{\text{molecule/surface}} - E_{\text{molecule}} - E_{\text{surface}}$$

where  $E_{\text{molecule/surface}}$  is the energy of the adsorption complex,  $E_{\text{molecule}}$  is the energy of the molecule in the gas phase, and  $E_{\text{surface}}$  is the energy of the clean surface. The most stable adsorption complex was further used to calculate the partial density of states (PDOS) and electron density difference (EDD).

### 3. Results and discussion

#### 3.1. Characterization of photocatalysts

The general crystallite size, microstructure and element mapping of the samples were characterized by TEM, high resolution TEM (HRTEM) and SEM-EDS. It's obvious that PT0 had larger crystallite size than commercial anatase TiO<sub>2</sub> and PT1 (Fig. 1a–c). The size distribution analysis was shown in Fig. S2, from which it can be seen that the mean

particle size was 5.77 nm, 12.93 nm and 6.97 nm for TiO<sub>2</sub>, PT0 and PT1 respectively. It is suggested that phosphate group would effectively hinder crystallites to agglomerate and further grow [33,50]. This demonstrated that TiO<sub>2</sub> was modified by phosphate group successfully and phosphate group could link firmly with the surfaces of the as-prepared crystallites [50]. Fig. 1d exhibited HRTEM image of PT1, in which the crystallite size was approximately 7 nm and a clear d-spacing of 0.35 nm obtained from PT1 was consistent with (101) planes of anatase TiO<sub>2</sub>. EDS mapping of PT1 indicated that element P was uniformly dispersed on the surface of TiO<sub>2</sub> (Fig. 1e–h).

The phase structures of the samples were analyzed by X-ray diffraction (XRD). As shown in Fig. 2a, several typical peaks at ca. 25.1°, 38.6°, 46.4° and 55.1° exhibited were crystallized in anatase phase (JCPDS No. 21-1272) [51,52]. It was seen that full width at half maximum of PT0 was smaller than any other modified samples, indicating it possessed better crystallinity and smaller crystallites. It's consistent with TEM results. Fig. 2b displayed the FT-IR spectra of PT0-PT2. The IR peaks at about 1630 and 3400 cm<sup>-1</sup> were ascribed to surface hydroxyl and adsorbed water molecules, respectively [53]. It was noticed that the phosphoric acid modified TiO<sub>2</sub> (PT0.1-PT2) had stronger IR peaks at about 1630 cm<sup>-1</sup>, which implied the higher amount of surface hydroxyl groups. This was favorable for generating hydroxyl radicals. In addition, the new peak appeared at about 1000–1200 cm<sup>-1</sup> representing the symmetric stretching mode of phosphate group [54]. X-ray photoelectron spectroscopy measurements (XPS) were performed for identifying the surface element chemical status of the photocatalysts, and the results are shown in Fig. 2c-d. The O1s peak of PT0 can be resolved into two peaks at about 530.07 eV and 531.73 eV, corresponding to the lattice oxygen of TiO<sub>2</sub> and oxygen of surface hydroxyl, respectively [55]. While the O1s of PT1 has three peaks at about 530.03 eV, 530.93 eV and 532.52 eV attributed to the lattice oxygen of

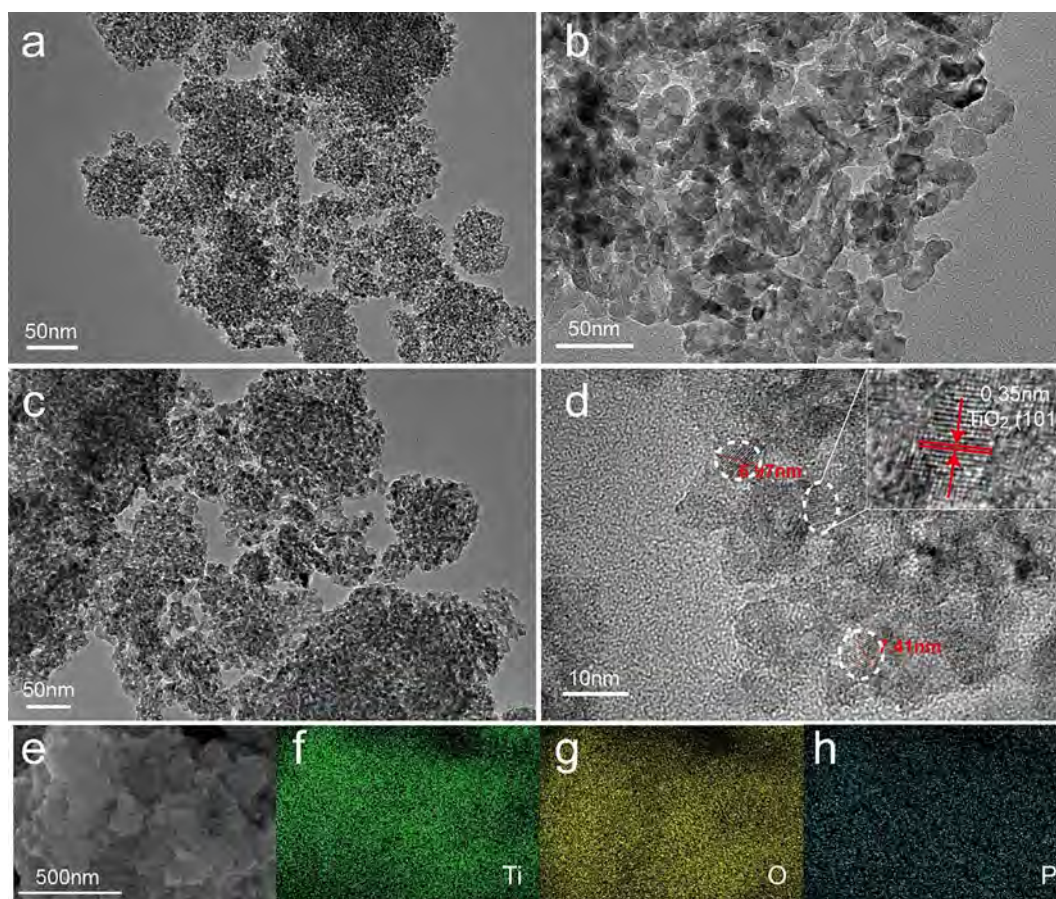


Fig. 1. TEM images of (a) commercial anatase TiO<sub>2</sub>, (b) PT0 and (c) PT1. HRTEM image of (d) PT1. (e) SEM and (f, g, h) EDS mapping images of PT1.

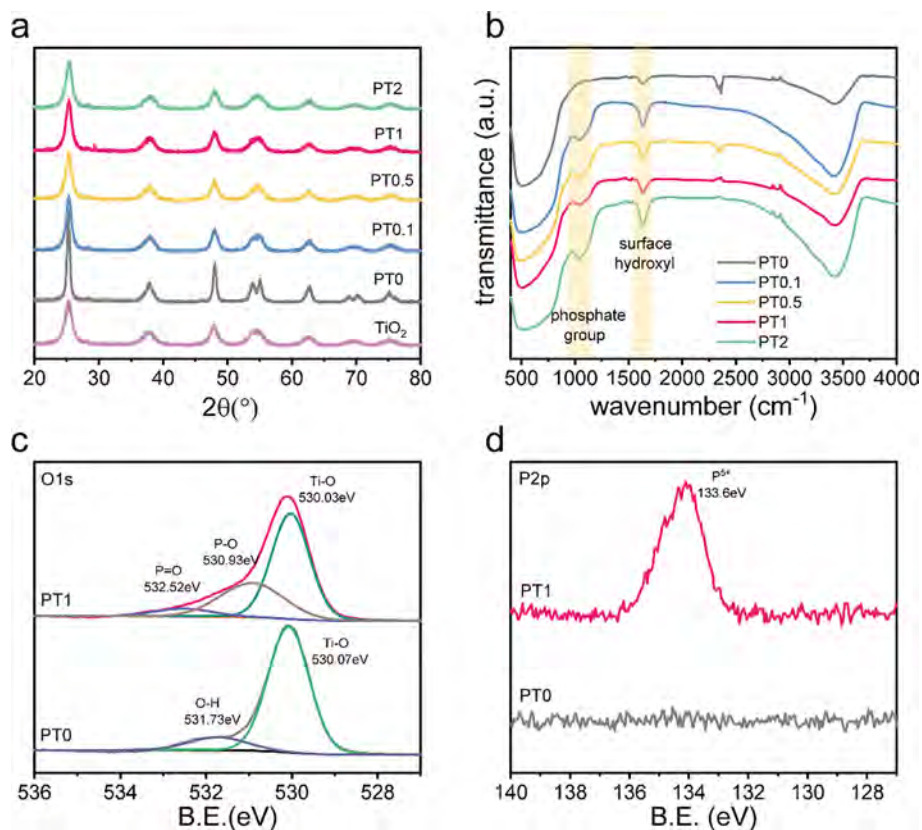


Fig. 2. (a) XRD patterns of TiO<sub>2</sub> and PT0-PT2. (b) FT-IR spectra of PT0-PT2. XPS spectra of (c) O1s and (d) P2p for PT1.

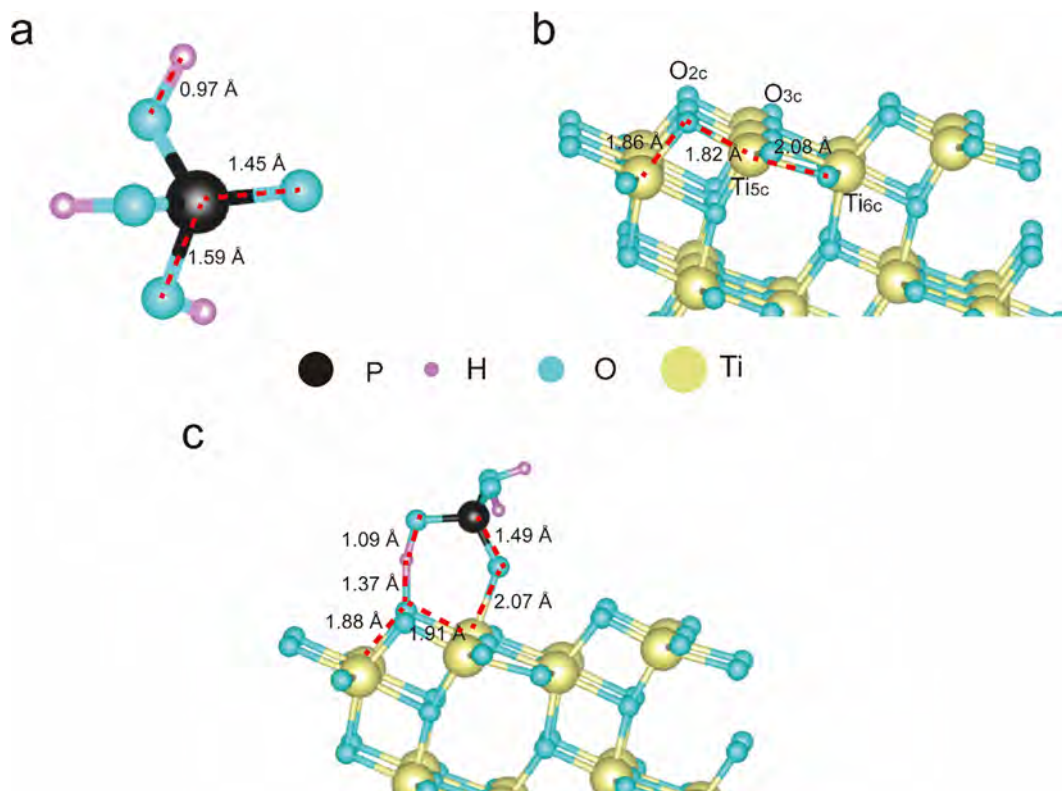


Fig. 3. Geometrically optimized structures for (a) phosphoric acid molecule and (b) (101) surface of anatase TiO<sub>2</sub>. (c) The most stable adsorption mode of phosphoric acid molecule on (101) surface.



TiO<sub>2</sub>, O (P–O or O–H) and O (P=O), respectively [56]. The P2p peak can be seen at about 133.6 eV, which is assigned to the P<sup>5+</sup> [57]. The surface atomic percentages for Ti, O, P and C were 22.55%, 57.18%, 2.45% and 17.83% respectively, which has been determined by XPS (see Table S1). Moreover, as shown in the Raman spectra of PT0 and PT1 (Fig. S3), the peak at 144 cm<sup>-1</sup> (e.g., symmetric stretching vibration of O–Ti–O of TiO<sub>2</sub>) shifted to a higher wave number, indicating phosphate absorbed on the surface strongly. These results demonstrated that the phosphate groups were anchored on the surface of TiO<sub>2</sub> successfully and the phosphate modification would have certain effects on the surface properties.

### 3.2. First principle calculations

Initially, the phosphoric acid molecule and anatase (101) surface were optimized to get a geometrically stable structure (Fig. 3a-b). After geometry optimization, the length of P=O, P–O and O–H bond have been calculated as 1.45 Å, 1.59 Å and 0.97 Å. The full relaxed anatase (101) surface was composed of 5-fold coordinated Ti atoms (Ti<sub>5c</sub>), 6-fold coordinated Ti atoms (Ti<sub>6c</sub>), 2-fold coordinated O atoms (O<sub>2c</sub>) and 3-fold coordinated O atoms (O<sub>3c</sub>). On the clean surface, the optimized Ti–O distances (Ti<sub>5c</sub>–O<sub>2c</sub>, Ti<sub>5c</sub>–O<sub>3c</sub> and Ti<sub>6c</sub>–O<sub>2c</sub>) were 1.82 Å, 2.08 Å and 1.86 Å, respectively, which was consistent with the previous report [58].

Phosphoric acid molecule or phosphate group adsorption on anatase (101) surface were studied. There were eight possible adsorption configurations with different adsorption energies calculated (Table 1). In the eight adsorption configurations (Fig. S4), p3 is the most stable one because of its highest exothermic adsorption energies. Fig. 3c showed p3 adsorption configuration with H(H<sub>3</sub>PO<sub>4</sub>)–O<sub>2c</sub> and =O(H<sub>3</sub>PO<sub>4</sub>)–Ti<sub>5c</sub> bond formed, of which the lengths are 1.37 and 2.07 Å, respectively. It can be clearly seen that there was structural deformation of lattice structure on the surface as well as phosphoric acid molecule. For example, the Ti<sub>5c</sub>–O<sub>2c</sub> and Ti<sub>6c</sub>–O<sub>2c</sub> bond length are larger than before (1.82 to 1.91 Å, 1.86 to 1.88 Å). The P=O and O–H bond of phosphoric acid molecule are elongated (1.45 to 1.49 Å, 0.97 to 1.09 Å). These results demonstrated p3 adsorption configuration could be the most probable adsorption on the surface and phosphoric acid molecule is chemically adsorbed through chemical bond formation (H(H<sub>3</sub>PO<sub>4</sub>)–O<sub>2c</sub> and =O(H<sub>3</sub>PO<sub>4</sub>)–Ti<sub>5c</sub> bond). These results suggested the phosphoric acid molecules would be captured by anatase (101) surface effectively and anchored on the surface by chemisorption.

To further understand adsorption mechanism of H<sub>3</sub>PO<sub>4</sub> on anatase (101) surface, we calculated the local density of states (LDOS) and charge density difference of adsorption mode p3 (Fig. 4). The total LDOS for phosphoric acid molecule adsorbed on anatase was shown in Fig. 4a, which demonstrated that p states and d states are the main contributors for VB and CB of the complex structure. The PDOS for Ti<sub>5c</sub>, O<sub>2c</sub>, =O and H was given in Fig. 4b–e. It was observed that VB maximum (VBM) mainly consisted of O2p from surface O and molecule =O. Whereas the CB minimum (CBM) mainly consisted of Ti 3d. Moreover, PDOS for Ti (Fig. 4b) and =O (Fig. 4d) experienced significant change in shape and intensity in contrast to Ti in clean surface (Fig. S5a) and =O in gas phase molecule (Fig. S5b), which indicated coupling between Ti and =O states. In addition, PDOS for surface O (Fig. 4c) and molecule H (Fig. 4e) had obvious broaden peaks, compared with O in clean surface (Fig. S5c) and H in gas phase molecule (Fig. S5d), which also confirmed strong interaction between surface O and molecule H. These results were consistent with the above

discussion on adsorption configurations. Electron density difference (EDD) was displayed in Fig. 4f, which presented the change of electron distribution. The green and yellow part represented electron-rich and the electron depleting region respectively. It was observed that the electron density near surface O<sub>2c</sub> and molecule =O increased, which indicated they tended to receive electrons. Whereas the electron density near molecule H and surface Ti<sub>5c</sub> decreased, suggesting they tended to lose electron. As a result, the strong chemical adsorption between H<sub>3</sub>PO<sub>4</sub> molecule and TiO<sub>2</sub> (101) formed, leading to favorable charge transfer. This result was also in good agreement with the optimized adsorption result.

### 3.3. Optical, photoelectrical and adsorption properties

From above results, it was demonstrated that phosphoric acid was modified on anatase TiO<sub>2</sub> (101) surface successfully and strong interaction between them was formed by chemical bond (H(H<sub>3</sub>PO<sub>4</sub>)–O<sub>2c</sub> and =O(H<sub>3</sub>PO<sub>4</sub>)–Ti<sub>5c</sub> bond). Therefore, to investigate the influence of this modification to optical, band structure, photoelectrical and adsorption properties, UV-vis, VB-XPS, PL, photocurrent response, electrochemical impedance, temperature-programmed desorption (TPD) and dark adsorption of samples were measured. Firstly, UV-vis absorption spectra were shown in Fig. 5a, presenting no significant difference between PT0 and PT1. The band gap calculated from the Kubelka-Munk function [59] (inset of Fig. 5a) were 3.02 and 2.95 eV for PT0 and PT1, respectively. These results implied phosphoric acid modification would not influence the optical property and band gap significantly. Even though it would not influence the band gap, it would change the VB maximum (VBM) position from +2.90 to +3.12 eV, which were measured by the VB X-ray photoelectron spectra (Fig. 5b). According to the formula of E<sub>CB</sub> = E<sub>VB</sub> – E<sub>g</sub>, the corresponding CB minimum (CBM) position of PT0 and PT1 would be located at ca. –0.12, +0.17 eV, respectively. Combined with the above results, the well-matched band structure of PT0 and PT1 was illustrated in Fig. 5c. It displayed the VBM and CBM were shifted to more positive potential, which would promote generation of hydroxyl radicals (·OH) and inhibit generation of superoxide (·O<sub>2</sub><sup>-</sup>) [60]. Photoelectrons generation, separation, and transmission are crucial for photocatalytic reactions. Fig. 5d showed the photoluminescence (PL) spectra of samples under the excitation wavelength of 320 nm. A strong PL peak represents a higher chance of recombination between electrons and holes. Obviously, the intensity of the PL peak for PT0.5 and PT1 was lower than that for PT0, indicating a lower recombination rate of photogenerated electrons and holes in the phosphoric acid modified TiO<sub>2</sub>. The photocurrent response of samples as measured under all spectrum light illumination (on-off interval of 10 s). Generally, the higher photocurrent response means the higher charge carrier density and more efficient charge carrier separation. As shown in Fig. 5e, PT0.5 and PT1 have higher photocurrent response than PT0, indicating the superior charge carrier separation and transmission properties in the phosphoric acid modified TiO<sub>2</sub>. In addition, electrochemical impedance spectra (EIS) was also utilized to probe the separation efficiency of charge carrier. As shown by the EIS Nyquist plots (Fig. 5f), the arc radii of PT0.5 or PT1 was smaller than that of PT0, indicating lower resistance and improved charge transfer ability of PT1. This is consistent with the above PL spectra and photocurrent response results.

Temperature-programmed desorption (TPD) and dark adsorption measurements were utilized to characterize the adsorption properties of samples for gaseous o-xylene. The higher intensity of desorption peak

**Table 1**  
Adsorption energies of phosphoric acid molecule on anatase (101) surface.

Adsorption configuration	p1	p2	p3	p4	p5	p6	p7	p8
E <sub>ad</sub> (eV)	-0.436	-0.216	-0.726	-0.404	-0.643	-0.581	17.568	17.584

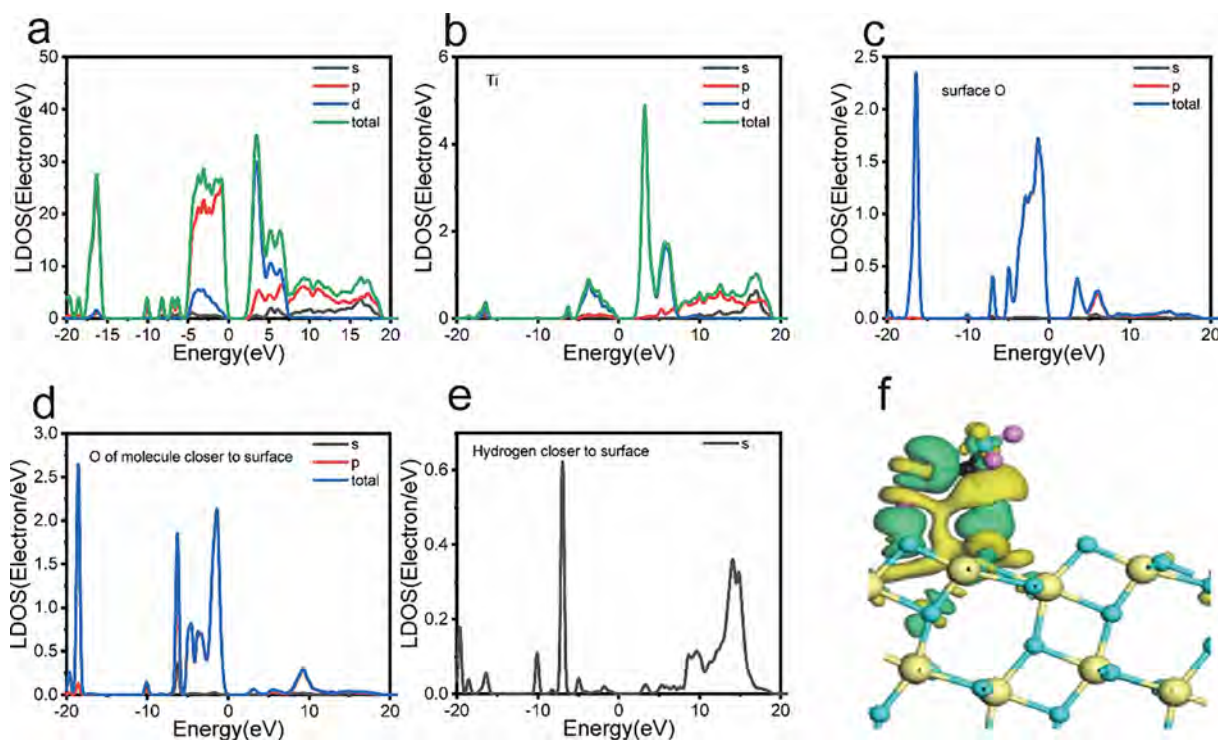


Fig. 4. Local density of states: (a) phosphoric acid molecule adsorbed on anatase, (b)  $Ti_{5c}$  and (c)  $O_{2c}$  of (101) surface; (d) =O and (e) H of phosphoric acid molecule. (f) charge density difference for the most stable adsorption mode (p3).

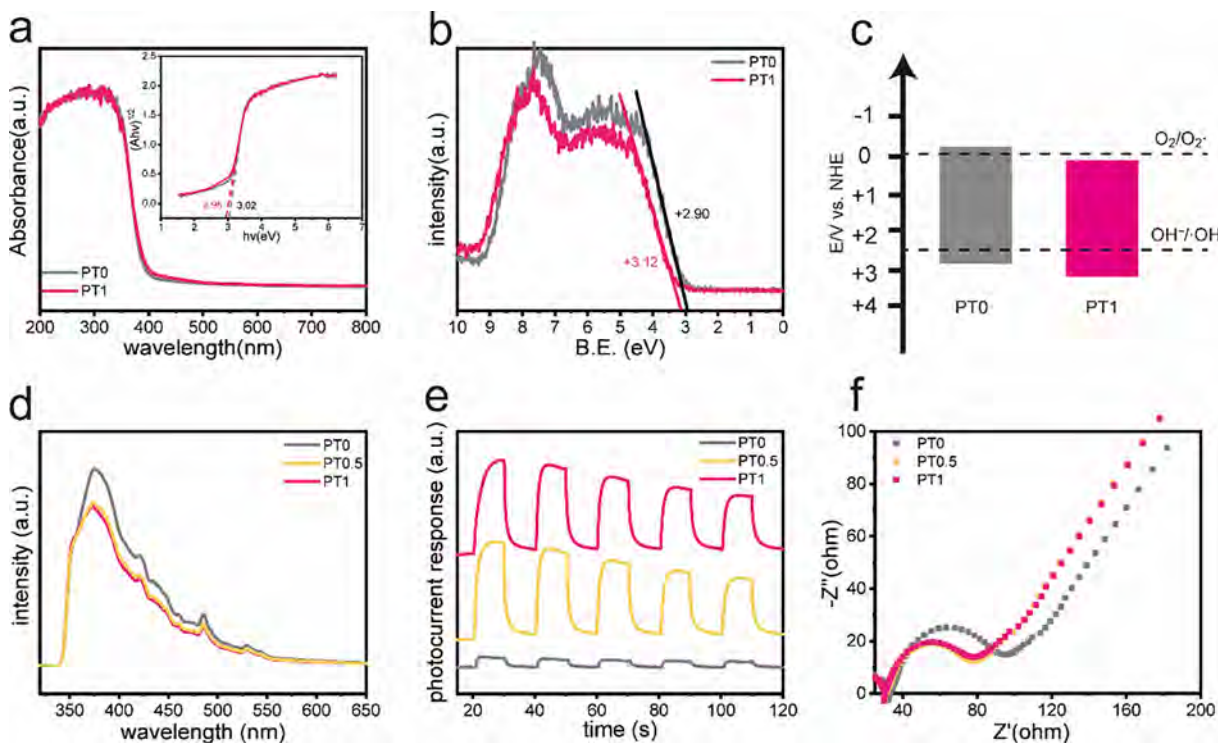


Fig. 5. (a) UV-vis absorption spectra and corresponding Tauc plot (inset of (a)). (b) Valence-band XPS spectra and (c) schematic of the band structures. (d) PL spectra, (e) photocurrent response and (f) Electrochemical impedance spectra (EIS) Nyquist plots of the as-prepared photocatalysts.

means that more gaseous molecules are adsorbed. As shown in Fig. 6a, the intensity of desorption peaks of PT1 was higher than that of PT0, suggesting that PT1 are capable of adsorbing more gaseous o-xylene and the change of desorption temperature could change the molecules adsorption configuration on the surface. This could be beneficial to the subsequent photocatalytic degradation reaction. The dynamic dark

adsorption could also reflect the adsorption performance. As shown in Fig. 6b, the maximal adsorption percent of gaseous o-xylene are 55% and 68% by PT0 and PT1 respectively. The final adsorption equilibrium of gaseous o-xylene was obtained in 140 min for PT0, while PT1 obtained the final adsorption equilibrium in 130 min. The results indicated that o-xylene adsorption by PT1 was more favorable than

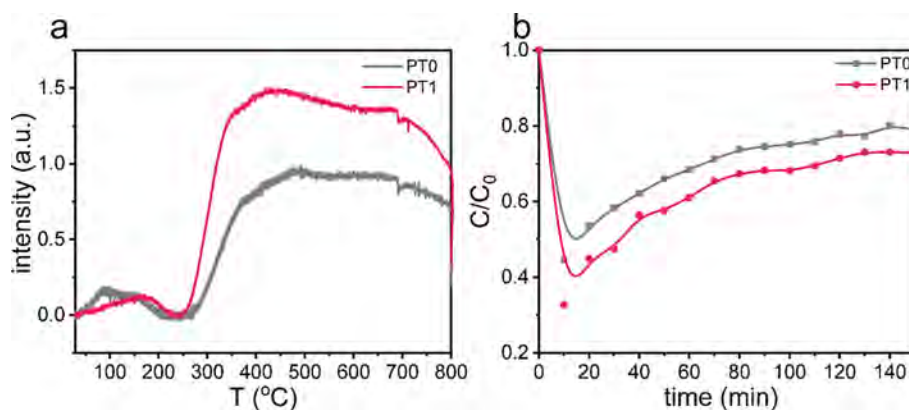


Fig. 6. (a) Temperature-programmed desorption (TPD) and (b) dark adsorption of PT0 and PT1 for gaseous o-xylene.

unmodified PT0, which was consistent with the above TPD results.

#### 3.4. Photocatalytic degradation of gaseous o-xylene and degradation intermediates

The photocatalytic degradation of gaseous o-xylene for all the samples were evaluated (Fig. 7a). It was obvious that there was no significant degradation by photolysis (blank). Moreover, the phosphoric acid modified TiO<sub>2</sub> samples displayed higher photocatalytic degradation activities compared to commercial TiO<sub>2</sub> (TiO<sub>2</sub>) and unmodified TiO<sub>2</sub> (PT0). Specifically (Fig. 7b), with TiO<sub>2</sub> and PT0 used as the photocatalysts, the conversion of o-xylene was 54.5% and 40.3% after 60 min of irradiation respectively. However, when PT1 was used as the photocatalyst, the removal efficiency was improved to 91.2%, indicating its excellent photocatalytic performance. However, if the surface phosphoric acid amount continued to increase, the activity would begin to go down. The excess surface phosphoric acid would be not favorable for the charge transportation mainly from one light-irradiating side along the particle to another no-light side or to different surface positions in the same particle, leading to a decreased charge separation and then to a low photocatalytic activity [30]. In addition, the photocatalytic degradation was reported to proceed via a pseudo-first order reaction with a Langmuir-Hinshelwood model when the initial concentration (C<sub>0</sub>) of pollutant is small. The simulation equation was expressed by the following equation:  $\ln(C_0/C) = kt$ , where C is the concentration of gaseous o-xylene at time t, C<sub>0</sub> is the initial concentration after equilibrium adsorption, and k (min<sup>-1</sup>) is the apparent first-order reaction rate constant [61]. The apparent rate constants were calculated and the results were shown in Fig. 7c, the k values were 0.0135 min<sup>-1</sup>, 0.00903 min<sup>-1</sup>, 0.0282 min<sup>-1</sup>, 0.0371 min<sup>-1</sup>, 0.0427 min<sup>-1</sup> and 0.0321 min<sup>-1</sup> for TiO<sub>2</sub>, PT0, PT0.1, PT0.5, PT1 and PT2, respectively. The PT1 exhibited the highest degradation rate,

which was approximately 3.2 times and 4.7 times as high as that of TiO<sub>2</sub> and PT0 respectively. For PT1, the simulation equation was also expressed by the following equation (Langmuir-Hinshelwood model):  $r = -\frac{dc}{dt} = \frac{kKC}{1+KC}$ , where k is the reaction rate constant (ppm·min<sup>-1</sup>); K is the adsorption constant (ppm<sup>-1</sup>); C is the o-xylene concentration in the gas phase (ppm); and r is the reaction rate (ppm·min<sup>-1</sup>). The inverse rate 1/r versus the inverse concentration 1/C should be linear:  $\frac{1}{r} = \frac{1}{kK} + \frac{1}{k}$ . It can be seen from Fig. S6 that the experimental data are in good agreement with this assumption. It was therefore verified the suitability of the Langmuir-Hinshelwood model. Value of the constant k was given in Fig. S6. As discussed above, we concluded that the phosphoric acid modification played a vital role in enhancing photocatalytic degradation of gaseous o-xylene. Based on the above results, the possible reasons were as follows: (i) the introduction of phosphoric acid chemisorbed onto TiO<sub>2</sub> surface led to the formation of strong acid sites [62–64] or anion-induced negative electrostatic field [29,65], which promoted separation and transfer of photogenerated electrons and holes; and (ii) the specific surface area of PT1 increased markedly (Table S2), as compared to that of PT0, which facilitated the access to adsorption sites as well as catalytic sites during the photocatalytic reaction. We further studied the stability and reusability of samples (Fig. S7). As shown in Fig. S7a, PT1 deactivated more easily compared with PT0, suggesting there might be more intermediates deposited on the modified surface. However, after four cycles, there are still over 85% of efficiency for o-xylene removal and phosphorus demonstrating good reusability (Fig. S7b). In addition, after 120 min degradation, there was no pronounced difference at about 1000–1200 cm<sup>-1</sup> showing good surface composition stability of PT1 (Fig. S7c).

During the photocatalytic degradation process, as the structure of gaseous o-xylene molecule was decomposed, some intermediate products on the PT0 and PT1 surface were generated. The main intermediate products were identified by GC-MS. The retention time (min),

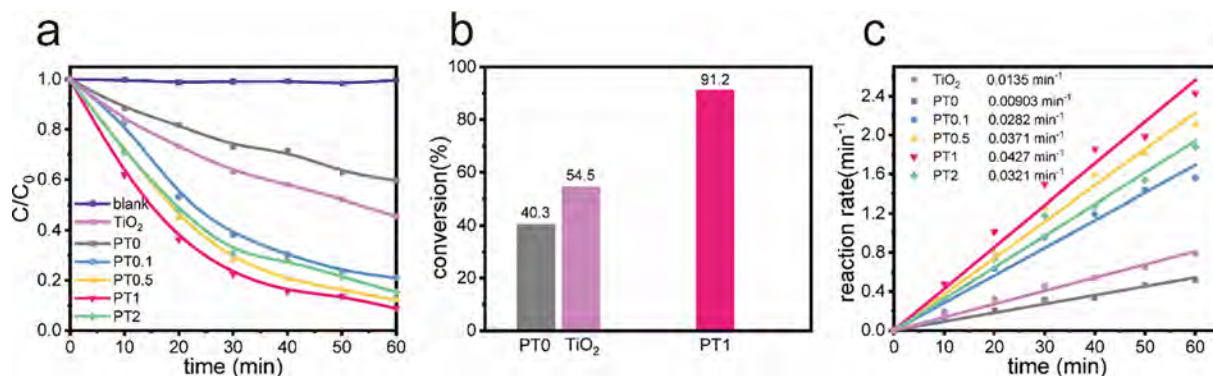
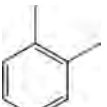
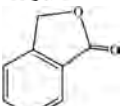
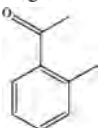
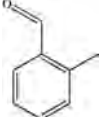
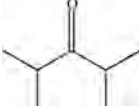
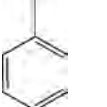
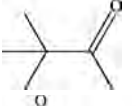
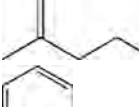
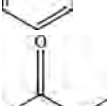

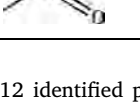
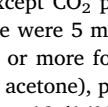


Fig. 7. (a) Photocatalytic degradation of gaseous o-xylene as a function of irradiation time under 300 W Xenon lamp irradiation, (b) comparison of conversion efficiency of TiO<sub>2</sub>, PT0 and PT1 and (c) Corresponding pseudo-first-order kinetic model of samples.



**Table 2**  
Identification of the photodegradation intermediates of o-xylene by GC-MS.

Product	Retention time/min	m/z	Structure formula
1	5.10	91,106,77	
2	11.05	105,77,134	
3	8.68	119,91,134	
4	7.75	91,119,65	
5	3.69	43,71,114	
6	3.36	91,92,65	
7	2.77	43,60,72	
8	2.57	43,86,71	
9	2.36	78,86,134	
10	1.96	43,58,59	
11	1.60	43,72,86	
12	1.45	44,56	

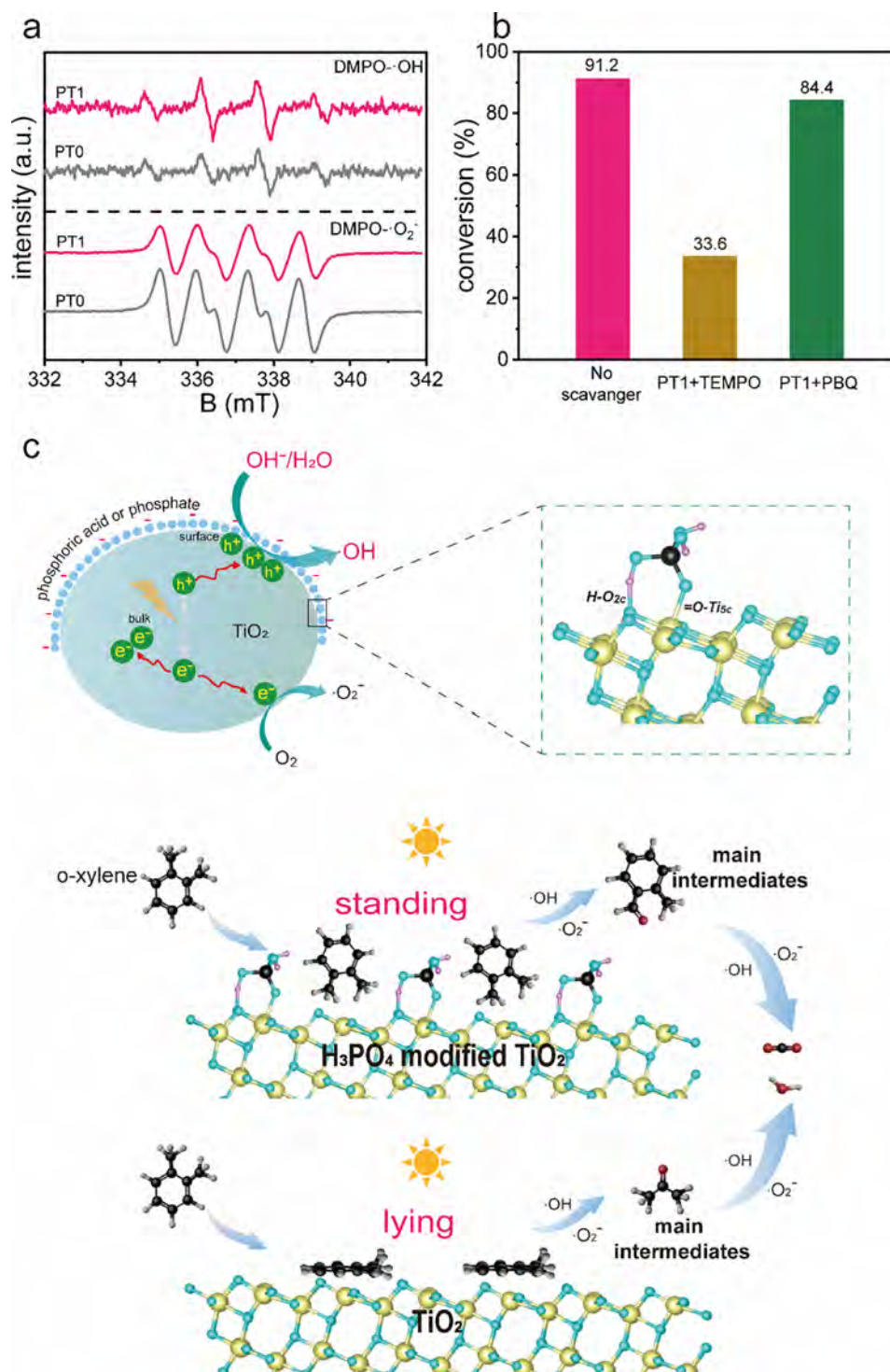
molecular ion (m/z), and structure formula of the 12 identified products are listed in Table 2. As shown in Fig. S8, except CO<sub>2</sub> peak at 1.38 min of retention time, it was obvious that there were 5 main intermediates peaks with a relative abundance of 1% or more for both PT0 and PT1. For PT0, they were product 11 (100%, acetone), product 9 (16%, butanone), product 6 (15%, toluene), product 12 (14%, acetaldehyde) and product 4 (4%, o-methyl benzaldehyde). For PT1, they were product 4 (100%, o-methyl benzaldehyde), product 11 (37%, acetone), product 6 (14%, toluene), product 12 (10%, acetaldehyde) and product 9 (5%, butanone). 100% means that acetone and o-methyl benzaldehyde are most abundant intermediates for PT0 and PT1 respectively. Other values represent abundance relative to acetone or o-methyl benzaldehyde. Hence, the relative abundance of intermediates changed after surface modification, indicating surface modification by phosphoric acid could influence surface reaction process of o-xylene. Generally, methyl oxidation, benzene-ring opening and subsequent

mineralization might be the three main reaction routes for o-xylene degradation [66–69]. Therefore, the intermediates (mainly o-methyl benzaldehyde and toluene) were primarily derived from the methyl oxidation reactions, followed by the open-ring reactions of the benzene ring to form smaller organic molecules (ketones and aldehydes, mainly acetone, butanone and acetaldehyde). Then these small organic molecules were further oxidized to CO<sub>2</sub> and H<sub>2</sub>O. As shown in Fig. S9, the CO<sub>2</sub> yield of PT1 for degrading o-xylene, monitored by gas chromatography equipped with a flame ionization detector and methane reforming furnace, was supplied. The selectivity of CO<sub>2</sub> was estimated as 53.8% using formula [70]:  $\frac{CO_{2out} - CO_{2in}}{8 \times RE(\%) \times C_{in}} \times 10000$ , where CO<sub>2</sub> in and CO<sub>2</sub> out represent the inlet and outlet concentrations of CO<sub>2</sub>, C<sub>in</sub> represents the inlet concentration of o-xylene and RE(%) represents removal efficiency of o-xylene.

### 3.5. Possible photocatalytic mechanism

Generally, it is accepted that VOCs are degraded mainly through reacting with photogenerated reactive oxygen species (ROS), such as superoxide ( $\cdot O_2^-$ ), hydroxyl radical ( $\cdot OH$ ) [71,72]. Therefore, to further explore the reaction mechanism beneficial for in-depth understanding the photocatalytic degradation of gaseous o-xylene, electron spin resonance (ESR) measurements and scavenger experiments were conducted to evaluate the ability of samples to produce  $\cdot O_2^-$  and  $\cdot OH$  and their roles in photocatalytic process. The ESR signals of DMPO- $\cdot O_2^-$  and DMPO- $\cdot OH$  were displayed in Fig. 8a, the DMPO- $\cdot OH$  signals of PT1 were stronger than that of PT0, whereas the DMPO- $\cdot O_2^-$  signals of PT1 were weaker than that of PT0. It meant that the phosphoric acid modification would enhance  $\cdot OH$  generation and inhibit  $\cdot O_2^-$  generation, which might be related to that the VBM and CBM were shifted to more positive potential (Fig. 5c). The scavenger experiments result was shown in Fig. 8b. The photodegradation efficiency of gaseous o-xylene was slightly depressed with the addition of PBQ ( $\cdot O_2^-$  scavenger), whereas an obvious drop was observed when the TEMPO ( $\cdot OH$  scavenger) was introduced. Consequently, it could be inferred that the produced  $\cdot OH$  was the dominant ROS in the photocatalytic degradation of gaseous o-xylene.

The possible mechanism of gaseous o-xylene photocatalytic degradation by phosphoric acid modified TiO<sub>2</sub> was illustrated in Fig. 8c. Under simulated sunlight irradiation, phosphoric acid modified absorbs photons generating electron-hole pairs. The introduction of phosphoric acid chemisorbed onto TiO<sub>2</sub> surface (H-O<sub>2</sub>C and =O-Ti<sub>5</sub>C chemical bonds) induces strong acid sites or negative electrostatic field, which is favorable to the access of photogenerated holes to the surface. Then the holes react with water or surface hydroxyl (-OH) to form hydroxyl radicals ( $\cdot OH$ ). The photogenerated electrons tend to move toward the bulk rather than the surface after surface phosphoric acid modification. But photogenerated electrons might be scavenged by oxygen (O<sub>2</sub>) on unmodified area, resulting in production of  $\cdot O_2^-$  radicals. These radicals attack o-xylene molecules in the close vicinity. Then the intermediates (mainly o-methyl benzaldehyde and toluene) derived from the methyl oxidation reactions are generated, followed by the open-ring reactions of the benzene ring to form smaller organic molecules (mainly acetone, butanone and acetaldehyde). Then these small organic molecules were further oxidized to CO<sub>2</sub> and H<sub>2</sub>O. Acetone and o-methyl benzaldehyde are the most abundant intermediates during o-xylene degradation for PT0 and PT1, respectively, which might be ascribed to the difference of surface adsorption configuration of o-xylene [73,74] and surface radicals generation [72,75]. Based on the ESR results (Fig. 8a), there is no big difference between surface radical generation. According to TPD results (Fig. 6a), the change of desorption temperature of PT0 and PT1 suggested surface modified by phosphoric acid could change the o-xylene adsorption configuration. Hence, it is inferred that surface modified by phosphoric acid changed the o-xylene adsorption configuration (from lying to standing on the surface) to



**Fig. 8.** (a) Superoxide ( $\cdot\text{O}_2^-$ ) signal with DMPO as scavenger in ethanol and hydroxyl radicals ( $\cdot\text{OH}$ ) signal with DMPO as scavenger in water. (b) Scavenger experiments using PBQ and TEMPO as corresponding  $\cdot\text{O}_2^-$  and  $\cdot\text{OH}$  scavenger. (c) Schematic diagram of possible mechanism of gaseous o-xylene photocatalytic degradation.

favor its methyl oxidation.

#### 4. Conclusions

In summary, TiO<sub>2</sub> surface modification by phosphoric acid was successfully synthesized for photocatalytic degradation of gaseous o-xylene under simulated sunlight irradiation. The PT1 showed superior photocatalytic degradation activity (91.2% in 60 min) and reaction rate ( $0.0427 \text{ min}^{-1}$ , 3.2 times and 4.7 times of TiO<sub>2</sub> and PT0). The reasons

for the enhancement were as follows: (i) the introduction of phosphoric acid chemisorbed onto TiO<sub>2</sub> surface (forming H-O<sub>2</sub>C and =O-Ti<sub>5</sub>C chemical bonds) led to the formation of strong acid sites or anion-induced negative electrostatic field, which inhibited recombination of photogenerated electrons and holes; and (ii) the specific surface area of PT1 increased markedly, which facilitated the access to adsorption sites as well as catalytic sites during the photocatalytic reaction. In addition, the possible reaction process was proposed. Firstly, the o-xylene was oxidized into intermediates (mainly o-methyl benzaldehyde and

toluene) derived from the methyl oxidation reactions, followed by the open-ring reactions of the benzene ring to form smaller organic molecules (ketones and aldehydes, mainly acetone, butanone and acetaldehyde). Then these small organic molecules were further oxidized to CO<sub>2</sub> and H<sub>2</sub>O. For PT0, relative abundance order of intermediates is acetone (67.1%) > butanone (10.7%) > toluene (10.1%) > acetaldehyde (9.4%) > o-methyl benzaldehyde (2.7%). Whereas for PT1, it is o-methyl benzaldehyde (60.3%) > acetone (22.3%) > toluene (8.4%) > acetaldehyde (6.0%) > butanone (3.0%). The difference might be ascribed to the difference of surface adsorption configuration of o-xylene. The surface modified by phosphoric acid could change the o-xylene adsorption configuration (from lying to standing on the surface) to favor its methyl oxidation. The selectivity of CO<sub>2</sub> during the o-xylene degradation for PT1 was estimated as 53.8% and PT1 deactivated more easily compared with PT0. Considering the commercial utilization, the further optimization such as surface deactivation or intermediates control will be required in future research. It is hoped that our work could be helpful to understand the relevance of surface modification and photodegradation reaction pathway and further promote the design of efficient photocatalyst and the potential application of its VOCs removal.

### Declaration of Competing Interest

The authors declare that they have no known competing financial interests or personal relationships that could have appeared to influence the work reported in this paper.

### Acknowledgements

This work was financially supported by the National Key Research and Development Program of China (2016YFA0203000), the NSFC-DFG bilateral organization program (51761135107) and the National Natural Science Foundation of China (41907303).

### Appendix A. Supplementary data

Supplementary data to this article can be found online at <https://doi.org/10.1016/j.cej.2020.124723>.

### References

- [1] F.N. Aguero, B.P. Barbero, L. Gambaro, L.E. Cadus, Catalytic combustion of volatile organic compounds in binary mixtures over MnOx/Al<sub>2</sub>O<sub>3</sub> catalyst, *Appl. Catal. B Environ.* 91 (2009) 108–112.
- [2] R. Kostianen, Volatile organic compounds in the indoor air of normal and sick houses, *Atmos. Environ.* 29 (1995) 693–702.
- [3] S. Wang, L. Zhang, C. Long, A. Li, Enhanced adsorption and desorption of VOCs vapor on novel micro-mesoporous polymeric adsorbents, *J. Colloid. Interf. Sci.* 428 (2014) 185–190.
- [4] C. Dai, Y. Zhou, H. Peng, S. Huang, P. Qin, J. Zhang, Y. Yang, L. Luo, X. Zhang, Current progress in remediation of chlorinated volatile organic compounds: a review, *J. Ind. Eng. Chem.* 62 (2018) 106–119.
- [5] H.I. Kim, H.N. Kim, S. Weon, G.H. Moon, J.H. Kim, W. Choi, Robust co-catalytic performance of nanodiamonds loaded on WO<sub>3</sub> for the decomposition of volatile organic compounds under visible light, *ACS Catal.* 6 (2016) 8350–8360.
- [6] E. Dumont, G. Darracq, A. Couvert, C. Couriol, A. Amrane, D. Thomas, Y. Andres, P. Le Cloirec, VOC adsorption in a countercurrent packed-bed column using water/silicone oil mixtures: Influence of silicone oil volume fraction, *Chem. Eng. J.* 168 (2011) 241–248.
- [7] T.K. Poddar, K.K. Sirkar, A hybrid of vapor permeation and membrane-based absorption-stripping for VOC removal and recovery from gaseous emissions, *J. Membrane. Sci.* 132 (1997) 229–233.
- [8] H. Cheng, Y. Hu, J. Luo, D.A. Sabatini, Multipass membrane air-stripping (MAS) for removing volatile organic compounds (VOCs) from surfactant micellar solutions, *J. Hazard. Mater.* 170 (2009) 1070–1078.
- [9] H. Wang, W. Yang, P. Tian, J. Zhou, R. Tang, S. Wu, A highly active and anti-coking Pd-Pt/SiO<sub>2</sub> catalyst for catalytic combustion of toluene at low temperature, *Appl. Catal. A Gen.* 529 (2017) 60–67.
- [10] M. Piumetti, D. Fino, N. Russo, Mesoporous manganese oxides prepared by solution combustion synthesis as catalysts for the total oxidation of VOCs, *Appl. Catal. B Environ.* 163 (2015) 277–287.
- [11] H. Xiao, R. Liu, X. Zhao, J. Qu, Enhanced degradation of 2,4-dinitrotoluene by ozonation in the presence of manganese(II) and oxalic acid, *J. Mol. Catal. A Chem.* 286 (2008) 149–155.
- [12] P. Rybarczyk, B. Szulczynski, J. Gebicki, J. Hupka, Treatment of malodorous air in biotrickling filters: a review, *Biochem. Eng. J.* 141 (2019) 146–162.
- [13] S. Sultana, A.M. Vandembroucke, C. Leys, N. De Geyter, R. Morent, Abatement of VOCs with alternate adsorption and plasma-assisted regeneration: a review, *Catalysts* 5 (2015) 718–746.
- [14] A.A. Assadi, A. Bouzaza, D. Wolbert, Comparative study between laboratory and large pilot scales for VOCs removal from gas streams in continuous flow surface discharge plasma, *Chem. Eng. Res. Des.* 106 (2016) 308–314.
- [15] S. Suarez, I. Jansson, B. Ohtani, B. Sanchez, From titania nanoparticles to decahedral anatase particles: Photocatalytic activity of TiO<sub>2</sub>/zeolite hybrids for VOCs oxidation, *Catal. Today* 326 (2019) 2–7.
- [16] J. Morin, A. Gandolfo, B. Temime-Roussel, R. Strekowski, G. Brochard, V. Berge, S. Gligorovski, H. Worthama, Application of a mineral binder to reduce VOC emissions from indoor photocatalytic paints, *Build. Environ.* 156 (2019) 225–232.
- [17] O. Debono, V. Gaudion, N. Redon, N. Locoge, F. Thevenet, Photocatalytic treatment of VOC industrial emissions: IPA removal using a sensor-instrumented reactor, *Chem. Eng. J.* 353 (2018) 394–409.
- [18] J. Zhang, J.H. Bang, C. Tang, P.V. Kamat, Tailored TiO<sub>2</sub>-SrTiO<sub>3</sub> heterostructure nanotube arrays for improved photoelectrochemical performance, *ACS Nano* 4 (2010) 387–395.
- [19] H.G. Yang, C.H. Sun, S.Z. Qiao, J. Zou, G. Liu, S.C. Smith, H.M. Cheng, G.Q. Lu, Anatase TiO<sub>2</sub> single crystals with a large percentage of reactive facets, *Nature* 453 (2008) 638–634.
- [20] X. Pan, M.-Q. Yang, X. Fu, N. Zhang, Y.-J. Xu, Defective TiO<sub>2</sub> with oxygen vacancies: synthesis, properties and photocatalytic applications, *Nanoscale* 5 (2013) 3601–3614.
- [21] X.Z. Li, F.B. Li, Study of Au/Au<sup>3+</sup>-TiO<sub>2</sub> photocatalysts toward visible photooxidation for water and wastewater treatment, *Enviro. Sci. Technol.* 35 (2001) 2381–2387.
- [22] S.U.M. Khan, M. Al Shahry, W.B. Ingler, Efficient photochemical water splitting by a chemically modified n-TiO<sub>2</sub>, *Science* 297 (2002) 2243–2245.
- [23] X. Chen, L. Liu, P.Y. Yu, S.S. Mao, Increasing solar absorption for photocatalysis with black hydrogenated titanium dioxide nanocrystals, *Science* 331 (2011) 746–750.
- [24] R. Asahi, T. Morikawa, T. Ohwaki, K. Aoki, Y. Taga, Visible-light photocatalysis in nitrogen-doped titanium oxides, *Science* 293 (2001) 269–271.
- [25] A. Matsuda, T. Matoda, Y. Kotani, T. Kogure, M. Tatsumisago, T. Minami, Evaluation of photocatalytic activity of transparent anatase nanocrystals-dispersed silica films prepared by the sol-gel process with hot water treatment, *J. Sol-Gel Sci. Technol.* 26 (2003) 517–521.
- [26] Y. Zhang, Z.-R. Tang, X. Fu, Y.-J. Xu, Nanocomposite of Ag-AgBr-TiO<sub>2</sub> as a photoactive and durable catalyst for degradation of volatile organic compounds in the gas phase, *Appl. Catal. B Environ.* 106 (2011) 445–452.
- [27] W.K. Jo, J.T. Kim, Application of visible-light photocatalysis with nitrogen-doped or unmodified titanium dioxide for control of indoor-level volatile organic compounds, *J. Hazard. Mater.* 164 (2009) 360–366.
- [28] A.H. Mamaghani, F. Haghghat, C.-S. Lee, Photocatalytic oxidation of MEK over hierarchical TiO<sub>2</sub> catalysts: Effect of photocatalyst features and operating conditions, *Appl. Catal. B Environ.* 251 (2019) 1–16.
- [29] H. Sheng, Q. Li, W. Ma, H. Ji, C. Chen, J. Zhao, Photocatalytic degradation of organic pollutants on surface anionized TiO<sub>2</sub>: common effect of anions for high hole-availability by water, *Appl. Catal. B Environ.* 138 (2013) 212–218.
- [30] Y. Cao, L. Jing, X. Shi, Y. Luan, J.R. Durrant, J. Tang, H. Fu, Enhanced photocatalytic activity of nc-TiO<sub>2</sub> by promoting photogenerated electrons captured by the adsorbed oxygen, *Phys. Chem. Chem. Phys.* 14 (2012) 8530–8536.
- [31] P.A. Connor, A.J. McQuillan, Phosphate adsorption onto TiO<sub>2</sub> from aqueous solutions: an in situ internal reflection infrared spectroscopic study, *Langmuir* 15 (1999) 2916–2921.
- [32] J. Kim, W. Choi, TiO<sub>2</sub> modified with both phosphate and platinum and its photocatalytic activities, *Appl. Catal. B Environ.* 106 (2011) 39–45.
- [33] X. Qin, L. Jing, G. Tian, Y. Qu, Y. Peng, Enhanced photocatalytic activity for degrading Rhodamine B solution of commercial Degussa P25 TiO<sub>2</sub> and its mechanisms, *J. Hazard. Mater.* 172 (2009) 1168–1174.
- [34] J. Bai, Y. Sun, M. Li, L. Yang, J. Li, The effect of phosphate modification on the photocatalytic H<sub>2</sub>O<sub>2</sub> production ability of g-C<sub>3</sub>N<sub>4</sub> catalyst prepared via acid-hydrothermal post-treatment, *Diam. Relat. Mater.* 87 (2018) 1–9.
- [35] S. Chen, R. Yan, X. Zhang, K. Hu, Z. Li, M. Humayun, Y. Qu, L. Jing, Photogenerated electron modulation to dominantly induce efficient 2,4-dichlorophenol degradation on BiOBr nanoplates with different phosphate modification, *Appl. Catal. B Environ.* 209 (2017) 320–328.
- [36] H. Cui, Y. Cao, L. Jing, Y. Luan, N. Li, Effects of inorganic acid modification on photocatalytic performance of TiO<sub>2</sub> and its activity-enhanced mechanism related to adsorbed O<sub>2</sub>, *Chempluschem* 79 (2014) 318–324.
- [37] J. Wu, H. Cui, X. Zhang, Y. Luan, L. Jing, Enhanced photocatalytic activity of Cl-residual rutile TiO<sub>2</sub> nanorods after targeted co-modification with phosphoric and boric acids, *Phys. Chem. Chem. Phys.* 17 (2015) 15837–15842.
- [38] L. Zhong, F. Haghghat, Photocatalytic air cleaners and materials technologies—abilities and limitations, *Build. Environ.* 91 (2015) 191–203.
- [39] A.H. Mamaghani, F. Haghghat, C.S. Lee, Photocatalytic oxidation technology for indoor environment air purification: the state-of-the-art, *Appl. Catal. B Environ.* 203 (2017) 247–269.
- [40] D.S. Muggli, J.T. McCue, J.L. Falconer, Mechanism of the photocatalytic oxidation of ethanol on TiO<sub>2</sub>, *J. Catal.* 173 (1998) 470–483.
- [41] V. Augugliaro, S. Coluccia, V. Loddo, L. Marchese, G. Martra, L. Palmisano,



- M. Schiavello, Photocatalytic oxidation of gaseous toluene on anatase TiO<sub>2</sub> catalyst: mechanistic aspects and FT-IR investigation, *Appl. Catal. B Environ.* 20 (1999) 15–27.
- [42] C. Yang, G. Miao, Y. Pi, Q. Xia, J. Wu, Z. Li, J. Xiao, Abatement of various types of VOCs by adsorption/catalytic oxidation: a review, *Chem. Eng. J.* 370 (2019) 1128–1153.
- [43] H. Sui, P. An, X. Li, S. Cong, L. He, Removal and recovery of o-xylene by silica gel using vacuum swing adsorption, *Chem. Eng. J.* 316 (2017) 232–242.
- [44] G. Kresse, J. Furthmuller, Efficiency of ab-initio total energy calculations for metals and semiconductors using a plane-wave basis set, *Comp. Mater. Sci.* 6 (1996) 15–50.
- [45] G. Kresse, J. Furthmuller, Efficient iterative schemes for ab initio total-energy calculations using a plane-wave basis set, *Phys. Rev. B* 54 (1996) 11169–11186.
- [46] J.P. Perdew, K. Burke, M. Ernzerhof, Generalized gradient approximation made simple (vol 77, pg 3865, 1996), *Phys. Rev. Lett.* 78 (1997) 1396.
- [47] Y. Lei, H. Liu, W. Xiao, First principles study of the size effect of TiO<sub>2</sub> anatase nanoparticles in dye-sensitized solar cell, *Model. Simul. Mater. Sci. Eng.* 18 (2010) 1–10.
- [48] J.K. Burdett, T. Hughbanks, G.J. Miller, J.W. Richardson, J.V. Smith, Structural electronic relationships in inorganic solids - powder neutron-diffraction studies of the rutile and anatase polymorphs of titanium-dioxide at 15 and 295K, *J. Am. Chem. Soc.* 109 (1987) 3639–3646.
- [49] S. Grimme, Semiempirical GGA-type density functional constructed with a long-range dispersion correction, *J. Comput. Chem.* 27 (2006) 1787–1799.
- [50] L. Jing, X. Qin, Y. Luan, Y. Qu, M. Xie, Synthesis of efficient TiO<sub>2</sub>-based photocatalysts by phosphate surface modification and the activity-enhanced mechanisms, *Appl. Surf. Sci.* 258 (2012) 3340–3349.
- [51] L. Nie, J. Yu, X. Li, B. Cheng, G. Liu, M. Jaroniec, Enhanced performance of NaOH-modified Pt/TiO<sub>2</sub> toward room temperature selective oxidation of formaldehyde, *Environ. Sci. Technol.* 47 (2013) 2777–2783.
- [52] W. Li, F. Wang, Y. Liu, J. Wang, J. Yang, L. Zhang, A.A. Elzatahry, D. Al Dahyan, Y. Xia, D. Zhao, General strategy to synthesize uniform mesoporous TiO<sub>2</sub>/Graphene/Mesoporous TiO<sub>2</sub> sandwich-like nanosheets for highly reversible lithium storage, *Nano Lett.* 15 (2015) 2186–2193.
- [53] Z. Ding, G.Q. Lu, P.F. Greenfield, Role of the crystallite phase of TiO<sub>2</sub> in heterogeneous photocatalysis for phenol oxidation in water, *J. Phys. Chem. B* 104 (2000) 4815–4820.
- [54] J.C. Yu, L.Z. Zhang, Z. Zheng, J.C. Zhao, Synthesis and characterization of phosphated mesoporous titanium dioxide with high photocatalytic activity, *Chem. Mater.* 15 (2003) 2280–2286.
- [55] S. Sodergren, H. Siegbahn, H. Rensmo, H. Lindstrom, A. Hagfeldt, S.E. Lindquist, Lithium intercalation in nanoporous anatase TiO<sub>2</sub> studied with XPS, *J. Phys. Chem. B* 101 (1997) 3087–3090.
- [56] M.C.O. Monteiro, G. Cha, P. Schmuki, M.S. Killian, Metal-phosphate bilayers for anatase surface modification, *ACS Appl. Mater. Inter.* 10 (2018) 6661–6672.
- [57] U. Ciesla, S. Schacht, G.D. Stucky, K.K. Unger, F. Schuth, Formation of a porous zirconium oxo phosphate with a high surface area by a surfactant-assisted synthesis, *Angew. Chem. Int. Edit.* 35 (1996) 541–543.
- [58] H. Liu, M. Zhao, Y. Lei, C. Pan, W. Xiao, Formaldehyde on TiO<sub>2</sub> anatase (101): a DFT study, *Comp. Mater. Sci.* 51 (2012) 389–395.
- [59] Y. Guo, P. Wang, J. Qian, Y. Ao, C. Wang, J. Hou, Phosphate group grafted twinned BiPO<sub>4</sub> with significantly enhanced photocatalytic activity: synergistic effect of improved charge separation efficiency and redox ability, *Appl. Catal. B Environ.* 234 (2018) 90–99.
- [60] X. Zeng, Z. Wang, G. Wang, T.R. Gengenbach, D.T. McCarthy, A. Deletic, J. Yu, X. Zhang, Highly dispersed TiO<sub>2</sub> nanocrystals and WO<sub>3</sub> nanorods on reduced graphene oxide: Z-scheme photocatalysis system for accelerated photocatalytic water disinfection, *Appl. Catal. B Environ.* 218 (2017) 163–173.
- [61] J. Sun, X. Li, Q. Zhao, J. Ke, D. Zhang, Novel V<sub>2</sub>O<sub>5</sub>/BiVO<sub>4</sub>/TiO<sub>2</sub> nanocomposites with high visible-light-induced photocatalytic activity for the degradation of toluene, *J. Phys. Chem. C* 118 (2014) 10113–10121.
- [62] X.C. Wang, J.C. Yu, P. Liu, X.X. Wang, W.Y. Su, X.Z. Fu, Probing of photocatalytic surface sites on SO<sub>4</sub><sup>2-</sup>/TiO<sub>2</sub> solid acids by in situ FT-IR spectroscopy and pyridine adsorption, *J. Photoch. Photobio. A Chem.* 179 (2006) 339–347.
- [63] X.C. Wang, J.C. Yu, Y.D. Hou, X.Z. Fu, Three-dimensionally ordered mesoporous molecular-sieve films as solid superacid photo catalysts, *Adv. Mater.* 17 (2005) 99+.
- [64] J. Huang, X. Wang, Y. Hou, X. Chen, L. Wu, X. Wang, X. Fu, Synthesis of functionalized mesoporous TiO<sub>2</sub> molecular sieves and their application in photocatalysis, *Micropor. Mesopor. Mater.* 110 (2008) 543–552.
- [65] D. Zhao, C. Chen, Y. Wang, H. Ji, W. Ma, L. Zang, J. Zhao, Surface modification of TiO<sub>2</sub> by phosphate: effect on photocatalytic activity and mechanism implication, *J. Phys. Chem. C* 112 (2008) 5993–6001.
- [66] M. Sleiman, P. Conchon, C. Ferronato, J.-M. Chovelon, Photocatalytic oxidation of toluene at indoor air levels (ppbv): towards a better assessment of conversion, reaction intermediates and mineralization, *Appl. Catal. B Environ.* 86 (2009) 159–165.
- [67] J. Meng, X. Wang, X. Yang, A. Hu, Y. Guo, Y. Yang, Enhanced gas-phase photocatalytic removal of aromatics over direct Z-scheme-dictated H<sub>3</sub>PW<sub>12</sub>O<sub>40</sub>/g-C<sub>3</sub>N<sub>4</sub> film-coated optical fibers, *Appl. Catal. B Environ.* 251 (2019) 168–180.
- [68] J. Li, X.A. Dong, G. Zhang, W. Cui, W. Cen, Z. Wu, S.C. Lee, F. Dong, Probing ring-opening pathways for efficient photocatalytic toluene decomposition, *J. Mater. Chem. A* 7 (2019) 3366–3374.
- [69] Y. Huang, S.S.H. Ho, Y. Lu, R. Niu, L. Xu, J. Cao, S. Lee, Removal of indoor volatile organic compounds via photocatalytic oxidation: a short review and prospect, *Molecules* 21 (2016).
- [70] W. Abou Saoud, A.A. Assadi, M. Guiza, A. Bouzaza, W. Aboussaoud, I. Soutrel, A. Ouederni, D. Wolbert, S. Rtimi, Abatement of ammonia and butyraldehyde under non-thermal plasma and photocatalysis: oxidation processes for the removal of mixture pollutants at pilot scale, *Chem. Eng. J.* 344 (2018) 165–172.
- [71] H. Wang, D. Yong, S. Chen, S. Jiang, X. Zhang, W. Shao, Q. Zhang, W. Yan, B. Pan, Y. Xie, Oxygen-vacancy-mediated exciton dissociation in BiOBr for boosting charge-carrier-involved molecular oxygen activation, *J. Am. Chem. Soc.* 140 (2018) 1760–1766.
- [72] P. Wei, D. Qin, J. Chen, Y. Li, M. Wen, Y. Ji, G. Li, T. An, Photocatalytic ozonation mechanism of gaseous n-hexane on MOx-TiO<sub>2</sub>-foam nickel composite (M = Cu, Mn, Ag): unveiling the role of OH and O<sub>2</sub><sup>-</sup>, *Environ. Sci. Nano* 6 (2019) 959–969.
- [73] K. Zhou, W. Ma, Z. Zeng, X. Ma, X. Xu, Y. Guo, H. Li, L. Li, Experimental and DFT study on the adsorption of VOCs on activated carbon/metal oxides composites, *Chem. Eng. J.* 372 (2019) 1122–1133.
- [74] H. Zhang, P. Zhou, H. Ji, W. Ma, C. Chen, J. Zhao, Enhancement of photocatalytic decarboxylation on TiO<sub>2</sub> by water-induced change in adsorption-mode, *Appl. Catal. B Environ.* 224 (2018) 376–382.
- [75] X. Sun, X. Luo, X. Zhang, J. Xie, S. Jin, H. Wang, X. Zheng, X. Wu, Y. Xie, Enhanced superoxide generation on defective surfaces for selective photooxidation, *J. Am. Chem. Soc.* 141 (2019) 3797–3801.